
Article:
Meo, A., Sampan-A-Pai, S., Visscher, P. B. et al. (6 more authors) (2021) Spin transfer torque switching dynamics in CoFeB/MgO magnetic tunnel junctions. Physical Review B. 054426. ISSN 2469-9969

https://doi.org/10.1103/PhysRevB.103.054426

Spin transfer torque switching dynamics in CoFeB/MgO magnetic tunnel junctions

A. Meo,[1,2,*] S. Sampan-a-pai,[2] P. B. Visscher,[3] R. Chepulskyy,[4] D. Apalkov,[4] J. Chureemart,[2] P. Chureemart,[2] R. W. Chantrell,[1] and R. F. L. Evans[1]

[1]*Department of Physics, University of York, York YO10 5DD, United Kingdom*
[2]*Department of Physics, Mahasarakham University, Mahasarakham 44150, Thailand*
[3]*Department of Physics and Astronomy, University of Alabama, Tuscaloosa, Alabama 35401, USA*
[4]*Samsung Semiconductor Inc., San Jose, California 95134, USA*

(Received 29 July 2020; revised 21 December 2020; accepted 3 February 2021; published 18 February 2021)

We perform atomistic simulations of spin transfer torque switching dynamics in CoFeB/MgO/CoFeB magnetic tunnel junctions. We base our study on Slonczewski's model parametrized following the approach of Zhang, Levy, and Fert. We utilize excitation modes and the contour integral of the magnetization to perform a deeper analysis of the switching mechanism driven by spin transfer torque. Our results show a magnetization reversal driven by the combination of coherent and nonuniform excitation modes. These can be nonuniform and initiated by a coherent mode of the magnetization, or domain wall nucleated depending on the lateral size, temperature, and current density injected into the system. Larger current densities result in stronger excitation of nonuniform modes making the switching more easily subjected to thermal excitations and structural imperfections such as edge damage. Our findings agree with experimental works on spin transfer torque switching in similar CoFeB/MgO-based systems, and they suggest the presence of complex features in the magnetization dynamics. The analysis and the results presented here can help to gain a deeper understanding of spin transfer torque dynamics in nanoscale devices.

DOI: 10.1103/PhysRevB.103.054426

I. INTRODUCTION

Spin transfer torque magnetic random access memories (STT MRAMs) are considered one of the most promising candidates to replace silicon-based memory technologies, in particular for applications that require low power consumption and moderate operational speed [1–3]. MRAMs are based on magnetic tunnel junctions (MTJs), which can be schematically described as a trilayer structure where two conducting ferromagnets are separated by an insulating nonmagnetic spacer. In MRAMs, the information is stored as magnetization polarization in one of the ferromagnets providing nonvolatility and hardness against electromagnetic disturbances [1–3]. In STT MRAMs, the writing process is achieved by exploiting, as the name suggests, the spin transfer torque phenomenon [4] that occurs in a ferromagnet when a flow of conducting electrons crosses the material and interacts with the local magnetization. If the density of these conducting electrons that have been previously spin-polarized by crossing the other ferromagnet is large, the torque exerted on the magnetization can induce a large precession of the latter that exceeds the natural precession yielding magnetization reversal [2,5]. For STT MRAMs to become a concrete alternative to the current memories, fast and reliable writing at low current densities is required. Therefore, a fundamental understanding of the mechanism by which the magnetization is reversed under the application of a spin-polarized current is of great interest.

The available models developed to describe the spin torque phenomenon typically rely on a continuum assumption that the magnetization varies smoothly with position [6–12]. When the system size approaches a few nanometers, the assumption of a continuous description of the system properties starts breaking down, and the discrete nature of the lattice cannot be neglected. At such nanoscopic lengthscales, the accurate treatment of interfaces, boundaries, and thermal effects [13] calls for the use of an atomistic approach to describe accurately the spin torque phenomenon. Here we model the spin-polarized induced switching dynamics based on Slonczewski's approach [4] parametrized following the spin accumulation model of Zhang, Levy, and Fert [14], adapting it to an atomistic level [15] to achieve a better understanding of the phenomenon in CoFeB/MgO-based MTJs.

II. METHODS

In this work, we use an atomistic spin model as implemented in the open source software package VAMPIRE [16,17]. The magnetization dynamics of the system is obtained by integrating the stochastic Landau-Lifshitz-Gilbert (sLLG) equation of motion applied at the atomistic level [18], of the form

$$\frac{d\vec{S}_i}{dt} = -\frac{\gamma}{(1+\alpha^2)}\left[\vec{S}_i \times \vec{\mathrm{H}}^i_{\mathrm{eff}} + \alpha\vec{S}_i \times \left(\vec{S}_i \times \vec{\mathrm{H}}^i_{\mathrm{eff}}\right)\right]. \quad (1)$$

$\vec{S}_i$ is the normalized unit spin vector on site i, $\gamma = 1.760\,86 \times 10^{11}\ \mathrm{s^{-1}\,T^{-1}}$ is the gyromagnetic ratio of the electron, and $\vec{\mathrm{H}}^i_{\mathrm{eff}}$ is the net effective field acting on the spin i,

*am1808@york.ac.uk; andrea.m@msu.ac.th

where

$$\vec{\mathrm{H}}^{i}_{\mathrm{eff}} = -\frac{1}{\mu^{i}_{\mathrm{s}}}\frac{\partial \mathscr{H}}{\partial \vec{S}_i} + \vec{\xi}_i. \tag{2}$$

The first term of Eq. (2) accounts for all the contributions in the localized extended Heisenberg Hamiltonian ($\mathscr{H}$):

$$\mathscr{H} = -\sum_{i<j} J_{ij}\vec{S}_i \cdot \vec{S}_j - \sum_i k^i_{\mathrm{u}}(\vec{S}_i \cdot \hat{e})^2 - \mu_0 \sum_i \mu^i_{\mathrm{s}}\vec{S}_i \cdot \vec{\mathrm{H}}_{\mathrm{app}} + \mathscr{H}_{\mathrm{dmg}}. \tag{3}$$

J_{ij} represents the exchange coupling constant between spin i and j, k^i_{u} is the uniaxial energy constant on site i along the easy-axis $\hat{e}$, μ^i_{s} is the atomic spin moment on the atomic site i, and $\vec{\mathrm{H}}_{\mathrm{app}}$ is the external applied field. The magnetostatic contributions $\mathscr{H}_{\mathrm{dmg}}$ are calculated using a modified macrocell approach [19]. This method accounts for the contribution within each cell explicitly computing the interaction tensor from the atomistic coordinates, following the work of Bowden [20]. This allows us to take into account the effect of different ferromagnetic layers in multilayer structures such as MTJs and spin valves. The second term of Eq. (2) couples the spin system with a heat bath. α is the atomistic Gilbert damping parameter that describes the relaxation of the atomic spins toward the direction of the effective field and includes the transfer of angular momentum within the same magnetic system via the excitation of propagating deviations in the ordering of the magnetic texture [21]. For the processes in which we are interested in this work, the magnetization dynamics occurs on the nanosecond timescale or slower. In this limit the thermal field $\vec{\xi}_i$ can be described by a Gaussian distribution in three dimensions, and the statistical moments of the distribution are found by applying the fluctuation theorem and the Fokker-Planck equation to obtain

$$\langle \xi_{i\alpha}(t)\rangle = 0, \tag{4}$$

$$\langle \xi_{ia}(t)\xi_{jb}(t\prime)\rangle = \frac{2\alpha k_{\mathrm{B}}T}{\mu_{\mathrm{s}}\gamma}\delta_{ij}\delta_{ab}\delta(t-t'), \tag{5}$$

where i, j label spins on the respective sites, $a, b = x, y, z$ are the vector components of $\vec{\xi}$ in Cartesian coordinates, t, t' are the times at which the Gaussian fluctuations are evaluated, T is the temperature, δ_{ij} and δ_{ab} are Kronecker deltas, and $\delta(t - t')$ is the Dirac delta function. Here α couples the spin system with the heat bath. We include the spin torque contribution as an additional term $\vec{\mathrm{H}}_{\mathrm{STT}}$ in $\vec{\mathrm{H}}_{\mathrm{eff}}$ basing our formalism on Slonczewski's approach [4] and following the work of Zhang *et al.* [14,22,23] to parametrize it:

$$\vec{\mathrm{H}}_{\mathrm{STT}} = a_{\mathrm{j_e}}\vec{S}_i \times \vec{\mathrm{M}}_{\mathrm{p}} + b_{\mathrm{j_e}}\vec{\mathrm{M}}_{\mathrm{p}}, \tag{6}$$

where $\vec{\mathrm{M}}_{\mathrm{p}}$ is the normalized unit vector describing the magnetization direction of the reference layer, and $a_{\mathrm{j_e}}$ and $b_{\mathrm{j_e}}$ are the dampinglike and fieldlike torque parameters, expressed in Tesla. They depend on the injected electrical current density and the structural, geometrical, and diffusive properties of the layers. The first term on the right-hand side (RHS) of Eq. (6) is due to the exchange interaction between the spin-polarized conduction electrons and the local moments within the ferromagnet, and it tends to align the conduction electrons along the magnetization direction. The second term is associated with the spatial mistracking of the conduction electrons and the local moments [24], spin flip scattering, and momentum transfer [25], although this term is still a subject of study [15]. Explicitly including $\vec{\mathrm{H}}_{\mathrm{STT}}$, the LLG equation reads

$$\frac{d\vec{S}_i}{dt} = -\frac{\gamma}{(1+\alpha^2)}\vec{S}_i \times \vec{\mathrm{H}}^{i}_{\mathrm{eff}} - \frac{\gamma\alpha}{(1+\alpha^2)}\left[\vec{S}_i \times \left(\vec{S}_i \times \vec{\mathrm{H}}^{i}_{\mathrm{eff}}\right)\right] - \frac{\gamma b_{\mathrm{j_e}}}{(1+\alpha^2)}\left(\vec{S}_i \times \vec{\mathrm{M}}_{\mathrm{p}}\right) + \frac{\gamma a_{\mathrm{j_e}}}{(1+\alpha^2)}\left[\vec{S}_i \times \left(\vec{S}_i \times \vec{\mathrm{M}}_{\mathrm{p}}\right)\right]. \tag{7}$$

The first two terms on the RHS of Eq. (7) are responsible for the damped precessional motion of the spins around the direction of the effective field $\vec{\mathrm{H}}^{i}_{\mathrm{eff}}$. The last two terms describe the effect of the spin torque on the spin motion due to an injected current. To obtain expressions for $a_{\mathrm{j_e}}$ and $b_{\mathrm{j_e}}$ we follow the approach discussed by Zhang *et al.* [14] for a trilayer magnetic system consisting of a reference ferromagnetic layer, a spacer, and a ferromagnetic layer with current injected perpendicular to the stack. In this model, the magnetization dynamics induced by spin-polarized current injected in a ferromagnet is described in terms of the interaction between the background magnetization and the local spin imbalance, called spin accumulation. This is achieved by coupling the dynamics of the spin accumulation and local moment in the ferromagnet within a spin diffusive framework. We point out that several assumptions have been made in Ref. [14] when determining the magnitude of $a_{\mathrm{j_e}}$ and $b_{\mathrm{j_e}}$ parameters. First, the barrier is assumed to be infinitely thin so that the polarization of the current is preserved during the crossing from one ferromagnet to the other. Second, the spin-dependent scattering at the interfaces is neglected, ensuring that all the current is absorbed and the reference layer is a half-metal, which yields full spin-polarization of the injected current density. In this work, we assume CoFeB is fully spin-polarized for the sake of simplicity, which also allows us to obtain a simple expression as in Ref. [14]. To further simplify the calculations, the limit $\lambda_{\mathrm{sf}} \gg \lambda_{\mathrm{J}}$ is taken, where λ_{sf} is the characteristic lengthscale over which the conduction electrons relax [14], and $\lambda_{\mathrm{J}} = \sqrt{2\hbar D_0/J_{\mathrm{sd}}}$ describes the lengthscale over which the spin-polarized electrons and the background moments interact. This depends on the diffusion constant of the free layer D_0 and the exchange coupling between the spin-polarized electrons and the magnetization J_{sd}. This assumption of $\lambda_{\mathrm{sf}} \gg \lambda_{\mathrm{J}}$, which holds for CoFeB/MgO systems in which $\lambda_{\mathrm{J}} \approx 3\,\mathrm{nm}$ and $\lambda_{\mathrm{sf}} \approx 15\,\mathrm{nm}$ [15,26], ensures that the polarization is conserved. In addition, the magnetization is supposed to be uniform within each magnetic layer, allowing each single layer to be described by a single macro spin, simplifying the discussion. Due to the atomistic nature of our calculations, we consider the contribution of each single atomic layer in the ferromagnets, and we obtain layer-resolved $a_{\mathrm{j_e}}$ and $b_{\mathrm{j_e}}$ parameters:

$$a_{\mathrm{j_e}}(z) = \frac{j_e\hbar a_0^3}{\sqrt{2}e\mu_{\mathrm{B}}\lambda_{\mathrm{J}}^2}\frac{1}{t_{\mathrm{l}}}\int_{z_{\mathrm{i}}}^{z_{\mathrm{f}}} dz\,\lambda_{\mathrm{J}}e^{-z\kappa}[\cos(z\kappa) + \sin(z\kappa)],$$

$$b_{\mathrm{j_e}}(z) = \frac{j_e\hbar a_0^3}{\sqrt{2}e\mu_{\mathrm{B}}\lambda_{\mathrm{J}}^2}\frac{1}{t_{\mathrm{l}}}\int_{z_{\mathrm{i}}}^{z_{\mathrm{f}}} dz\,\lambda_{\mathrm{J}}e^{-z\kappa}[\cos(z\kappa) - \sin(z\kappa)]. \tag{8}$$

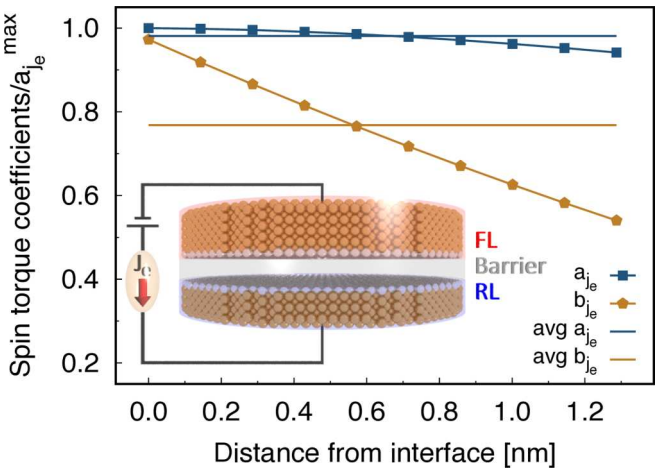

FIG. 1. Dependence on the distance from the interface of the spin torque coefficients normalized by the largest a_{j_e}, which occurs at the interface and is marked by thickness = 0, obtained integrating Eq. (8) for a MgO/CoFeB free layer of thickness 1.3 nm. Constant lines mark the average a_{j_e} and b_{j_e}. The inset shows a schematic of the investigated CoFeB/MgO/CoFeB MTJ, where silver spheres represent the high anisotropy interfacial layer, and gold spheres represent the bulklike CoFeB layers.

t_l is the thickness of a single atomic layer, z_i and z_f are the vertical coordinates of the atomic layer over which the integration is carried, a_0 is the lattice constant of the layer, $\hbar = 1.055 \times 10^{-34}$ J s is the reduced Planck constant, $e = 1.602 \times 10^{-19}$ C is the electron charge, $\mu_B = 9.274 \times 10^{-24}$ A m^2 is the Bohr magneton, and $\kappa = 1/(\sqrt{2}\lambda_J)$.

Figure 1 shows the dependence on the distance from the interface of a_{j_e} and b_{j_e} for a MgO/CoFeB free layer of thickness 1.3 nm, which corresponds to 10 atomic layers. A detailed parametrization will be discussed later in the text (see Table I). A value of zero on the x-axis marks the interface MgO/CoFeB. a_{j_e} and b_{j_e} are characterized by different thickness dependences: b_{j_e} decreases more rapidly and reaches almost 50% of its initial value, whereas the a_{j_e} remains almost constant throughout the thickness of 1.3 nm. As a comparison, the average values of a_{j_e} and b_{j_e} over the free layer thickness are plotted with lines. It is important to observe that the strength of both a_{j_e} and b_{j_e} are comparable close to the interface between the ferromagnet and the barrier, and therefore, even if b_{j_e} decays rapidly within the ferromagnet, the fieldlike torque should be taken into account in the dynamics of the magnetization. However, this contribution is often neglected [6,7,9–12]. With the layer-resolved spin torque parameters and the inclusion of the fieldlike term, an extra degree of information is added within the model with respect to a simple Slonczewski approach. Nonetheless, the torque is assumed uniform in each plane, an approximation that is not necessarily valid in finite systems.

TABLE I. Simulation parameters for the investigated systems.

	CoFeB (@interface)	CoFeB (bulk)	Unit
J_{ij}	1.547×10^{-20}	7.735×10^{-21}	J link^{-1}
μ_s	1.6	1.6	μ_B
k_u	1.35×10^{-22}	0.0	J atom^{-1}
α	0.11	0.003	

III. ANALYSIS OF THE SWITCHING MECHANISM

We will consider a thin cylindrical sample whose magnetization $\mathbf{M}(x, y)$ depends on the in-plane coordinates x and y, but is independent of z. In general, the reversal of nanoscale MRAM devices is a nonuniform process for devices larger than 20 nm in diameter [13]. In the following, we present two approaches to quantifying this nonuniformity for the analysis of the switching mechanism and spin wave excitations driven by spin transfer torque.

A. Contour integral

We will first give a method for using a contour integral to study inhomogeneities in the z-component $M_z(x, y)$ of the magnetization. A common way to quantify its variation with x and y is through its moments: the zeroth moment $m_z \equiv t \int M_z(x, y)dx\,dy$ (the integral is over a circle of radius R; the integral over z just gives a factor of the thickness t) and the two first moments

$$m_z^x \equiv t \int x M_z(x, y)dx\,dy, \quad m_z^y \equiv t \int y M_z(x, y)dx\,dy. \tag{9}$$

We compute these moments in our atomistic system by weighting the moment of each atom by its position coordinate x or y. The first moments give information about the variation of M_z across the disk. In particular, if the left side ($x < 0$) has $M_z = -M_s$ and the right side ($x > 0$) has $M_z = +M_s$, so that there is a domain wall at $x = 0$, then m_z^x will be positive. To deal with domain walls in other directions, it is useful to combine these first moments into a complex first moment,

$$\begin{aligned} m_z^x + i m_z^y &\equiv t \int (x + iy) M_z(x, y)dx\,dy \\ &= t \int_0^R dr \int_0^{2\pi} r e^{i\theta} M_z(x, y) r\,d\theta \\ &= t \int_0^R r dr \oint (-i) M_z(x, y)dc, \end{aligned} \tag{10}$$

where we have converted to polar coordinates and $c \equiv x + iy = re^{i\theta}$, $dc = ire^{i\theta}d\theta$; the contour integral is over a circle of radius r. Except for the factor of $-i$, this is the radial integral of a complex contour integral of the form $\oint M_z dc$, so we define a total contour integral

$$P_{\text{total}} \equiv t \int_0^R r\,dr \oint M_z(x, y)dc = i(m_z^x + i m_z^y). \tag{11}$$

It is clear from Eq. (10) that a rotation by an angle δ ($\theta \to \theta + \delta$) introduces a factor $e^{i\delta}$ into the moment or into P_{total}, so since P_{total} is purely imaginary for our domain wall along $x = 0$, the phase of P_{total} tells us the angle of the domain wall. The magnitude of P_{total} gives information about the position of the domain wall—if it is close to an edge (e.g., just nucleating) so that the number of overturned spins is small, then P_{total} will be small. It will be a maximum when the domain wall is at the

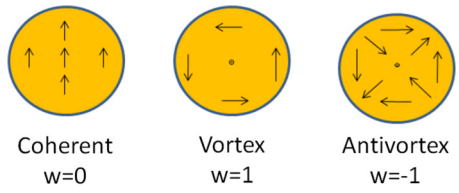

FIG. 2. Sketch of the lowest three normal modes of the cylinder, labeled by winding number w, from Visscher *et al.* [10].

center of the disk. To give further information about the radial position of the nonuniformities, we have subdivided P_{total} into contributions from N annuli: $P_1, P_2, \ldots, P_N$ are given by

$$P_n \equiv t \int_{(n-1)R/N}^{nR/N} r\,dr \oint M_z(x,y)dc. \tag{12}$$

Because the effects of edge nucleation are manifest first in the outermost annulus, the graphs in this paper show P_N.

B. Excitation modes

Visscher *et al.* [8,10] investigated the nature of the switching mechanism in cylindrical spin transfer torque MRAMs by means of micromagnetic simulations, and they based their analysis on the stability of the lowest frequency normal modes, which are a small perturbation of the equilibrium magnetic state. They classify these modes by the winding number w, an integer index that can be understood as the number of times the local magnetization winds around the disk axis as one travels around the disk once. The amplitudes of the three lowest-frequency modes ($w = 0, 1, -1$) can be expressed as [8,10]

$$\begin{aligned} m_0 &= \int (M_x + iM_y)dx\,dy, \\ m_1 &= \int [(xM_x + yM_y) + i(xM_y - yM_x)]dx\,dy, \\ m_{-1} &= \int [(xM_x - yM_y) + i(xM_y + yM_x)]dx\,dy, \end{aligned} \tag{13}$$

where (as before) the integral is over a circle of radius R. For the $w = 0$ mode, the magnetization is nearly independent of position [8], hence we refer to this as the uniform or "quasi-coherent" mode—this is the lowest energy mode. The other two modes represent the first excited states and are referred to as "vortex" ($w = 1$) and "antivortex" ($w = -1$). These three modes are sketched in Fig. 2.

IV. SYSTEM PROPERTIES

We study the switching dynamics in CoFeB/MgO/CoFeB MTJs induced by the application of a spin-polarized current as a function of diameter, applied current, and temperature. The inset of Fig. 1 presents a sketch of the investigated system. We parametrize CoFeB(1.0 nm,RL)/MgO(0.85 nm)/CoFeB(1.3 nm,FL) in the same way as was done in Ref. [13], where the number in parentheses is the thickness, and RL and FL refer to reference layer and free layer, respectively. We model CoFeB as cylindrical alloy films with a body-centered-cubic (bcc) crystal structure with lattice constant 2.86 Å. The CoFeB/MgO interface is characterized by a large perpendicular uniaxial single-ion anisotropy, about 1.1 mJm^{-2} for the free layer, whose value is obtained from anisotropy energy density temperature dependence measurements in CoFeB/MgO thin films performed by Sato *et al.* [27]. CoFeB atomic layers opposite to MgO are assumed to have no particular interfacial properties, and we neglect the small bulk anisotropy of CoFeB [28]. We use a mean-field approximation that depends on the Curie temperature T_c to extract the atomistic exchange parameters J_{ij}:

$$J_{ij} = \frac{3k_B T_c}{\varepsilon z}. \tag{14}$$

Here k_B is the Boltzmann constant, z are the nearest neighbors, and ε is the spin-wave excitation correction [17,29]. We impose that T_c must be the same in the whole CoFeB to extract interfacial and bulk J_{ij} values, where T_c is from CoFeB/MgO thin films measurements [27]. The corresponding exchange stiffness is obtained (it can be found in standard textbooks [30–32]) as $A_s(0\text{K}) = cJ_{ij}S^2/2a_0$, where S is the spin value, c is a factor depending on the crystal structure ($c = 2$ for a bcc structure), and a_0 is the lattice constant. We obtain 27 pJm^{-1} for both bulklike and interfacial CoFeB, a value close to experimental measurements on similar systems by Devolder *et al.* [33]. We assign an atomic spin moment μ_s of $1.6\mu_B$ to CoFeB, which corresponds to M_s about 1.3 MAm^{-1}, in agreement with experimental reports on similar systems [28]. We characterize the CoFeB/MgO interface with a larger damping than the rest of the CoFeB, in agreement with both experimental [28,34] and theoretical [35] works. Boron is not directly included in the simulations being nonmagnetic, however its effects are included in the anisotropy and atomic magnetic moment values. A list of the parameters used in our simulations can be found in Table I.

We initialize the system in an antiparallel state with the magnetization of the reference (free) layer pointing along the positive (negative) z-direction. We let the system equilibrate for one nanosecond to ensure a correct initial configuration. For simulations performed at $T = 0$ K, the free layer magnetization is misaligned by 1° from the z-axis to introduce an initial torque acting on the magnetization. Afterward, we apply the current to the free layer under the assumption that the electrons have been spin-polarized by the reference layer. In our study, we simulate MTJ diameters of 10, 20, 30, and 40 nm and different current densities j_e ranging from 7×10^{10} Am^{-2} $\times$ 10^{11} Am^{-2}. Such j_e values, despite being higher than those used in actual devices, allow us to capture the essential features without an excessive computational cost. Moreover, in the following we present and discuss only those systems that exhibit the most relevant features for the sake of clarity and brevity.

V. SWITCHING DYNAMICS

A. Dynamics in zero temperature

Figures 3(a) and 3(b) shows the time evolution of the reduced magnetization components of the free layer for a low current density $j_e = 1 \times 10^{11}$Am^{-2} at 0 K for device diameters of 20 and 30 nm, as obtained from atomistic simulations.

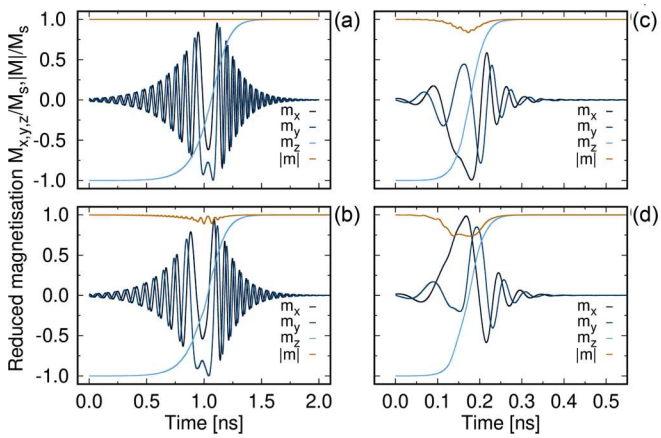

FIG. 3. Plot of the simulated switching dynamics of the free layer magnetization in CoFeB/MgO/CoFeB MTJ of diameter 20 nm (top figures) and 30 nm (bottom figures) MTJs for $j_e = 1 \times 10^{11}\mathrm{Am}^{-2}$ (left figures) and $j_e = 5 \times 10^{11}\mathrm{Am}^{-2}$ (right figures) at $T = 0$K. Different blue shades represent the x-, y-, and z-components of the magnetization $M_{x,y,z}/M_s$, whereas the reduced magnetization length $|\tilde{M}|/M_s = |m|$ is presented in brown.

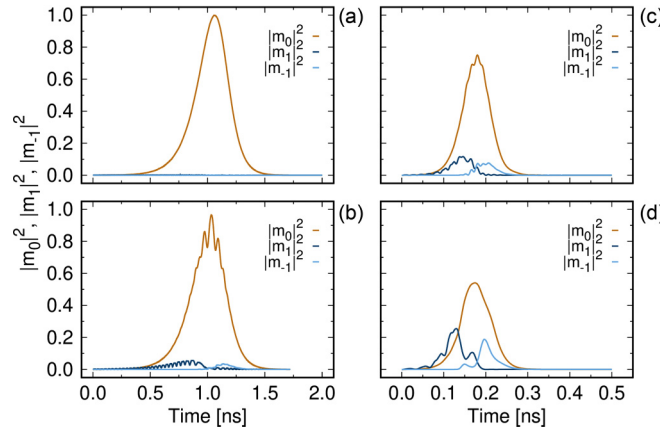

FIG. 4. Comparison of the calculated amplitudes of the excitation modes of the free layers of 20 nm (top figures) and 30 *nm* (bottom figures) MTJs for $j_e = 1 \times 10^{11}\mathrm{Am}^{-2}$ (left figures) and $j_e = 5 \times 10^{11}\mathrm{Am}^{-2}$ (right figures) at $T = 0$ K.

The reversal occurs in about a nanosecond and the in-plane components of the magnetization exhibit a character typical of uniform precession. Despite the coherent-like behavior, we observe nonuniform features in the magnetization length for diameters larger than 20 nm, where the magnetization length decreases and it exhibits oscillations superimposed on the main trend. When a larger j_e is applied the switching becomes faster, and nonuniform features are visible also at 20 nm, as shown in Fig. 3(c). The magnetization length decreases by 10% suggesting that the reversal mechanism is affected by the current density, with a transition from coherent to nonuniform switching. The drop in magnetization length increases with the diameter of the MTJ reaching nearly 30% for a diameter of 30 nm [Fig. 3(d)]. Moreover, by comparing Figs. 3(d) and 3(c), we can observe that this nonuniform feature lasts longer for the larger MTJ. This suggests that the magnetization dynamics for the same j_e becomes more complex as the diameter increases.

By studying the time evolution of the magnetization, we can obtain a general view of the spin transfer torque dynamics. To gain a deeper understanding regarding the dynamics and the nature of the reversal mechanism, we calculate the contour integral and the excitation modes of the magnetization. These analysis methods have been presented in Secs. III A and III B, respectively. In Fig. 4 we present a comparison of the calculated amplitudes of the excitation modes of the free layers of 20 nm (top figures) and 30 nm (bottom figures) MTJs for $j_e = 1 \times 10^{11}\mathrm{Am}^{-2}$ (left figures) and $j_e = 5 \times 10^{11}\mathrm{Am}^{-2}$ (right figures). For $j_e = 1 \times 10^{11}\mathrm{Am}^{-2}$ and diameter 20 nm the system presents the coherent mode only, hence the system behaves like a macrospin, as shown in panel (a) of Fig. 4. The spin configurations of the free layer in Fig. 5(a) confirm the coherent behavior and clearly show the rotational dynamics induced by the spin torque.

Analogous features are found for a smaller diameter. The analysis of Fig. 4(c) shows that as we increase j_e, the amplitude of m_0 decreases and is replaced by the nonuniform modes. Interestingly, we find that only either m_1 or m_{-1} is excited in turn and that a transition from one to the other occurs. This mode exchange cannot be explained only by the reversing of the winding direction of the in-plane components of the magnetization from clockwise to counterclockwise that occurs when the magnetization changes sign in a vortex, as this would not alter the vortex or antivortex structure sketched in Fig. 2. Nonetheless, this change in the winding rotation can be observed in the snapshots of the magnetization representing the in-plane components, as shown in Figs. 5(e)–5(h), as well as a superimposed coherent mode. We conclude that this transition between m_1 and m_{-1} excitation modes should be associated with a change in the symmetry of the reversal mechanism, although a full understanding has yet to be achieved. The analysis of the time evolution of the real and imaginary components of the contour integral for the most external annulus the disk is subdivided in, presented in Figs. 6(a) and 6(c), shows that the contour integral is zero for $j_e = 1 \times 10^{11}\mathrm{Am}^{-2}$, as expected for coherent reversal. On the other hand, when a higher current density is injected into the system, we observe oscillations of the real and imaginary part of the contour integral. The switching mechanism with the coexistence of a main coherent mode and a weaker nonuniform excitation is similar to that obtained by Visscher *et al.* [8,10]. However, in our case the rotation continues throughout the whole reversal process, whereas a linear propagation of the reversed region from one edge of the system to the other is found in Refs. [8,10]. The reason for the difference in the dynamics is still unclear, although we believe that the rotation of the in-plane components of the magnetization can be ascribed to the spin torque since it always has an in-plane component.

Figures 5(b) and 5(d) present the snapshots of the magnetization for a 30 nm MTJ. Differently from the smaller diameter, a noncoherent character can be observed even for the lowest j_e. The diameter is now comparable with its single domain size, and magnetic domains can now be introduced into the system. We can see strong similarities between panels (b) (30 nm, $1 \times 10^{11}\mathrm{Am}^{-2}$) and (c) (20 nm, $5 \times 10^{11}\mathrm{Am}^{-2}$).

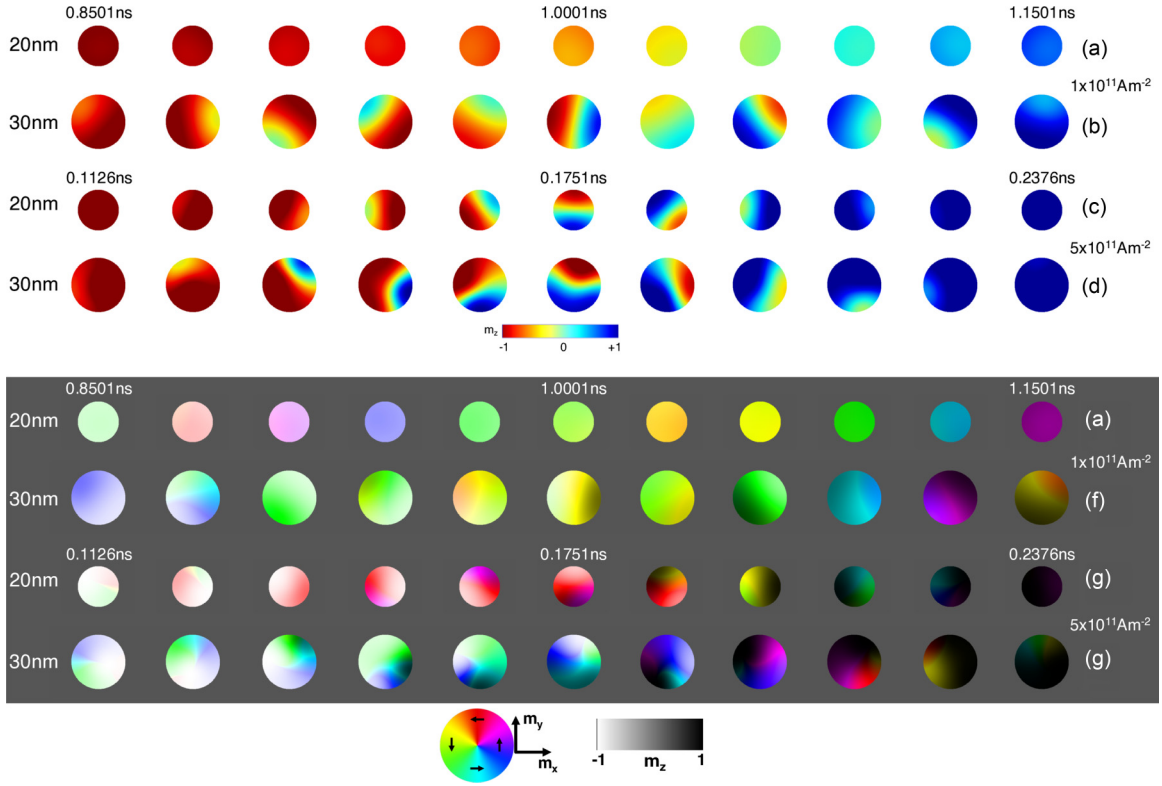

FIG. 5. Snapshots of spin transfer torque induced magnetization reversal at $T = 0\,\mathrm{K}$ for the free layer of a MTJ stack of diameter 20 nm [(a,e) and (c,g)] and 30 nm [(b,f) and (d,h)] for $j_e = 1 \times 10^{11}\mathrm{Am}^{-2}$[(a,e) and (b,f)] and $j_e = 5 \times 10^{11}\mathrm{Am}^{-2}$[(c,g) and (d,h)]. Snapshots from (a) to (d) describe the out-of-plane magnetization, and the color scheme represents the z component of the magnetization (blue for $+z$, red for $-z$, and green for $z = 0$). Snapshots from (e) to (h) describe the in-plane magnetization configuration with the hue representing the in-plane components of the magnetization and the intensity of the color the out-of-plane component. The timescale of the switching differs depending on the current density: around a nanosecond for $j_e = 1 \times 10^{11}\mathrm{Am}^{-2}$ and an order of magnitude less for $j_e = 5 \times 10^{11}\mathrm{Am}^{-2}$.

However, the domain wall exhibits breathinglike modes, and the reversal appears as quasicoherent close to the switching point in the larger system. Confirmation comes from the normal modes analysis. By comparing Figs. 4(b) and 4(c), we can see that in both cases m_0 remains the highest excited mode, and $m_{1,-1}$ have small amplitudes. Moreover, a transition from

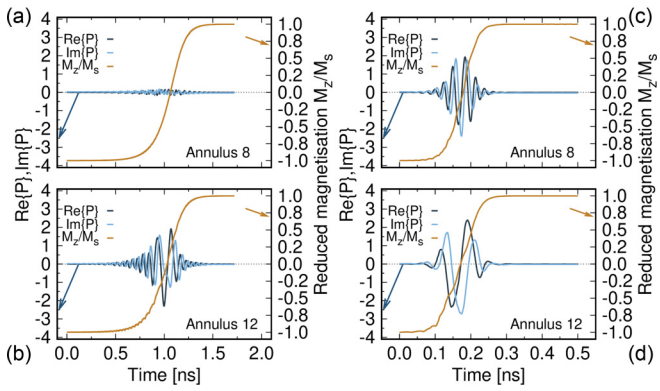

FIG. 6. Comparison of the calculated components of the contour integral of the magnetization for the most external annulus of the free layers of 20 nm (top figures) and 30 nm (bottom figures) MTJs for $j_e = 1 \times 10^{11}\mathrm{Am}^{-2}$ (left figures) and $j_e = 5 \times 10^{11}\mathrm{Am}^{-2}$ (right figures) at $T = 0\,\mathrm{K}$. The magnetization of the annulus is plotted in brown, and arrows indicate the y-axis of reference.

one to the other occurs close to the switching point. However, $m_{1,-1}$ have lower amplitudes and m_0 exhibits large oscillations close to the reversal in the larger MTJ. The latter is a result of the complex magnetization dynamics with the oscillations of m_0 that correspond to the breathinglike modes of the domain wall. The former suggests that the current density plays a major role in determining the mechanism of the magnetization reversal. The contour integral analysis of the most external region of the disk, shown in Fig. 6(b), suggests that the reversed region originates at the edge of the system. These nonuniform excitations induce an overall nonuniform switching, favored by the large in-plane size of the system.

A change in the dynamics occurs when we inject a higher current density, with the vortex mode m_1 initially excited and retaining an amplitude larger than m_0 for one-third of the switching event, depicted in Fig. 4(d). Differently from the previous cases, the domain wall width is constant during the reversal and thinner. This is supported by the absence of oscillations in the m_0 excitation mode observed for the lower j_e in Fig. 4(c). From the contour integral analysis, Fig. 6, we find a larger oscillation with a lower frequency in the real and imaginary components of the contour integral than observed previously. This confirms the stronger nonuniform character of the reversal as the diameter and j_e increase. Such a behavior is not ideal for applications, where uniform processes are desirable. Moreover, snapshots of the in-plane magnetization [Fig. 5(h)] show the formation of vortex-like spin structures

during the initial part of the reversal and antivortex-like states after the magnetization switches sign. It is still unclear what drives the transition from vortex to antivortex modes, and further investigation is required. In fact, this cannot be ascribed to a change in the magnetization sign since a simple magnetization reversal from $-z$ to $+z$ preserves the excitation modes.

It is worth noting that the reversal mechanism in zero temperature differs markedly from the dynamics induced by the application of an external field discussed in Ref. [13] by Meo *et al.* There the field normal to the disk and the magnetostatic field, which is stronger at the center of the disk, result in center nucleated dynamics for large enough diameters. In contrast, the in-plane component of the spin torque field aids nonuniformity at the edge of the system and can drive the formation of a reversed magnetized region. For small diameters, the reversal is coherent in both cases, although it is accompanied by rotation of the domain wall structure when the spin-polarized current is injected. Interestingly, a similar behavior to Ref. [13] is observed in zero-temperature micromagnetic simulations [8,11,12] until the magnetization switches its sign. We can attribute this difference in the magnetization dynamics to two factors: (i) the contribution arising from the fieldlike torque is neglected, and (ii) the magnetostatic interaction between FL and RL is not considered. The former introduces in-plane components that can favor nucleation of reversed magnetized regions. The latter can destabilize the magnetization of FL when the two layers are antiparallel, an effect that is stronger at the edges. In addition, atomistic models allow sharp variation of the magnetization, and therefore noncollinear magnetic configurations are more likely to occur.

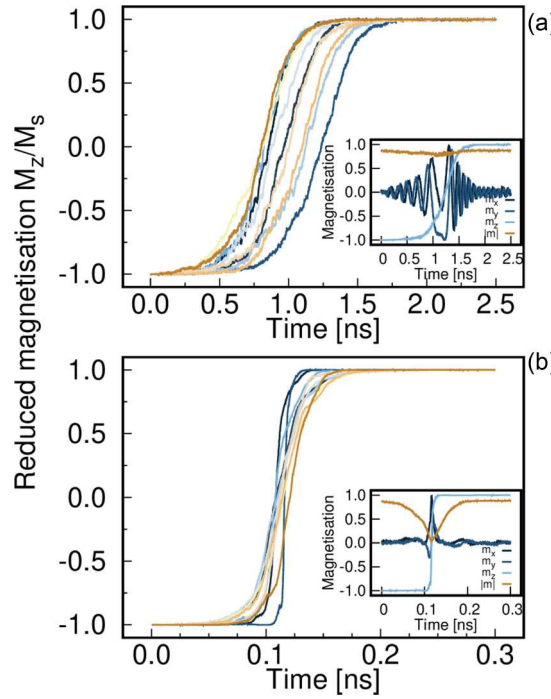

FIG. 7. Plot of the reduced z-component of the magnetization M_z/M_s of the free layer of CoFeB/MgO MTJs with diameter 30 nm obtained simulating ten independent switching events at $T = 300$ K for an injected current $j_e = 7 \times 10^{10}\mathrm{Am}^{-2}$ (a) and $j_e = 5 \times 10^{11}\mathrm{Am}^{-2}$ (b). Different colors refer to different runs. The insets show the reduced components of the magnetization for a specific switching event. Different blue shades represent the x-, y-, and z-components of the magnetization $M_{x,y,z}/M_s$, whereas the reduced magnetization length $|\vec{M}|/M_s = |m|$ is presented in brown.

B. Effect of temperature

The analysis of the reversal mechanism induced by spin-polarized currents developed so far neglects thermal effects. We expect that the random fluctuations might yield a stochastic character to the reversal, leading to faster switching due to thermal activation. They might also affect the nature of the magnetization dynamics, similar to the case of field-induced magnetization dynamics [13]. Toward this aim, we simulate the spin transfer torque dynamics at a temperature of 300 K. We let the system equilibrate for 1 ns to ensure that we start from a state that is at thermal equilibrium. We simulate ten different switching events using a different pseudo-random-number sequence that represents the random nature of the thermal noise to obtain a statistical average over the switching times.

The reversal becomes nonuniform for diameters larger than 10 nm even for the lowest j_e due to the thermal activation. Random thermal agitation promotes nucleation sites at the edge of the system, where spins suffer from reduced exchange links, favoring nonuniform processes. To illustrate the thermal effects on the switching properties, we present here the dynamics for the lowest ($7 \times 10^{10}\mathrm{Am}^{-2}$) and highest ($5 \times 10^{11}\mathrm{Am}^{-2}$) investigated current densities j_e. These represent the two extremes and allow us to discuss the most relevant effects induced by thermal fluctuations. Similarly, we focus on a diameter dimension (30 nm) where such effects are more visible. Figure 7 presents the time evolution of the reduced z-component of the magnetization M_z/M_s of the free layer of a 30 nm MTJ for different j_e. For the low current density, there is a large distribution of magnetization curves over time (i.e., switching time), whereas the switching of the magnetization does not exhibit significant differences for different runs. The time evolution of the magnetization shows a reversal that originates at the edge of FL, as observed at low temperature. Differently from the low-temperature case in which the current-induced switching differs markedly from the field-induced simulations, the origin of the reversal is edge nucleated in both approaches at finite temperature. The different propagation of the domain wall across the disk between field-induced and spin transfer torque-induced switching can be attributed to the symmetry of the spin transfer torque that is responsible for the rotational behavior.

M_z/M_s exhibits a narrower distribution when $j_e = 5 \times 10^{11}\mathrm{Am}^{-2}$ is applied, and, interestingly, the transition of M_z/M_s during the reversal is particularly sharp in some of the simulations. One of these cases is shown in the inset of Fig. 7(b). Here we do not observe rotation of the in-plane components of the magnetization, a characteristic feature observed so far and expected from spin torque dynamics. In addition, the free layer almost completely demagnetizes at the switching point, then recovering the magnetization as the dynamics proceeds. We compute the excitation modes associated with

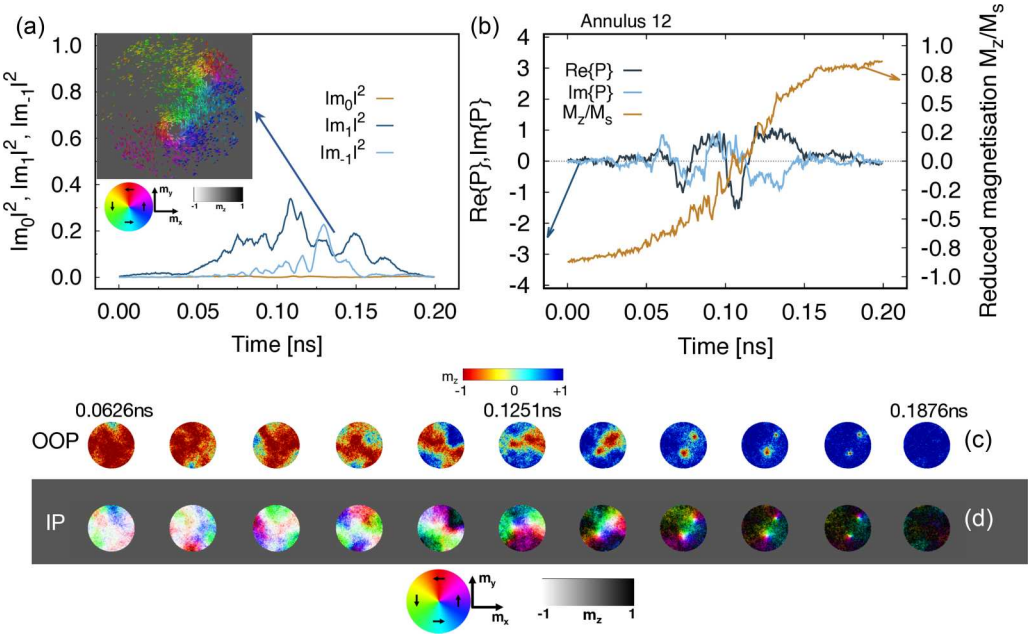

FIG. 8. (a) Calculated amplitudes of the excitation modes and (b) components of the contour integral of the magnetization for the most external annulus of the free layers of 30 nm MTJs whose magnetization dynamics is presented in the inset of Fig. 7(b), and arrows indicate the respective y-axis of the integral components. The time evolution of the spin configuration for the same system is presented in (c) (out-of-plane) and (d) (in-plane), where the color scheme is the same as previously described. The inset in (a) shows the in-plane spin configuration when the peak of the m_{-1} mode occurs.

this switching event and the contour integral of the magnetization, shown in Figs. 8(a) and 8(b), respectively. Surprisingly, the coherent mode m_0 is suppressed, with m_1 the most strongly excited mode throughout the dynamics. We do not observe the usual transition from vortex to antivortex mode. Instead m_{-1} exhibits only a peak around the switching. The analysis of the real and imaginary components of the contour integral does not show the usual oscillatory behavior, and we do not find large variations as a function of radius. This confirms that the mechanism differs from edge nucleation in these cases. The snapshots of the spin configurations suggest the simultaneous formation and coexistence of metastable vortex- and antivortex-like states, which must be responsible for the peak of m_{-1} observed in the excitation modes' time dependence, shown in the inset of Fig. 8(a). The spin configurations of Figs. 8(c) and 8(d) show that the nonreversed regions, a vortex and an antivortex, shrink until they disappear. Such a behavior can occur in an atomistic model, whereas in a continuous model these topologically protected singularities would have to merge and annihilate. Since these switching events are observed at finite temperature only, they must be the effect of the stochastic nature of the reversal coupled with the symmetry of the spin torque field components together with the large injected j_e. The switching of the larger diameters exhibits similar properties to those described above and are not shown here. All these features confirm the complex character of the reversal dynamics driven by the random nature of the thermal fluctuations and the need for a further understanding of the switching dynamics at finite temperature in these systems.

We extract the mean switching times and their distributions from the simulated time dependence of the z-component of the magnetization. In this work, we separate the switching time in two components: a "transient time" required to initiate the reversal, and a "reversal time" during which the magnetization is reversed, as sketched in the inset of Fig. 9(b).

The transient time is taken as the time from the start of the simulation until the z-component of the magnetization decreases by 10% in its magnitude, while the reversal time corresponds to the time during which the z-component of the magnetization varies by 80% after the end of the transient time. The total switching time is obtained as the sum of transient and reversal times. We compare the size dependence of the transient and reversal times in Figs. 9(a) and 9(b) at zero temperature and $T = 300$ K for two different j_e. We expect the reversal time to be a characteristic property of the system, and as such to depend on j_e and not particularly on the temperature. The extracted mean reversal times plotted in Fig. 9(b) are comparable at $T = 0$ and 300 K, supporting our thesis that the reversal is determined by the material properties of the system. On the other hand, the transient time exhibits a clear dependence on size and temperature, as can be observed in Fig. 9(a). For small j_e at $T = 300$ K, the average reversal time decreases with the MTJ diameter. At finite temperature, small diameters become thermally unstable and the switching can be initiated before, in analogy with the coercive field dependence on the junction diameter at high temperature [13]. As we inject higher current densities, this effect persists, but it is mitigated by the larger effective field acting on the system. We focus on the distribution of switching times. We find that the reversal time distribution is weakly dependent on the size and current density. The distribution is around 0.03 ns and it can be seen as a further confirmation of the intrinsic nature of the reversal time. The transient time is characterized by a larger distribution around 0.1 ns for small j_e, whereas the

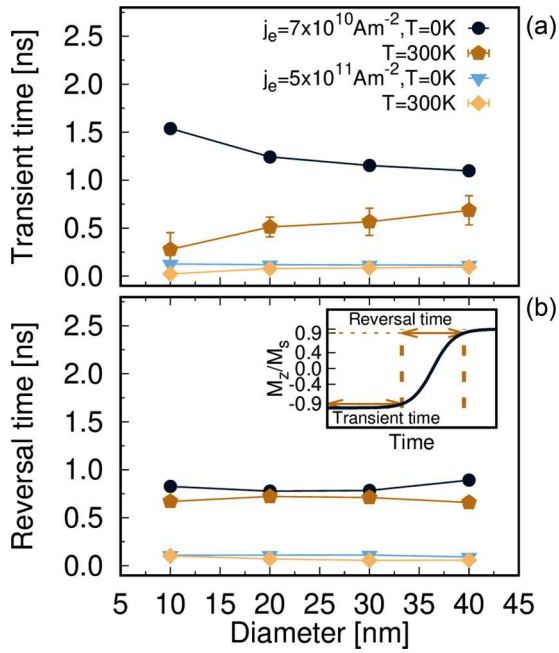

FIG. 9. Plot of the calculated mean transient (a) and reversal (b) switching times of the free layer magnetization induced by spin transfer torque dynamics as a function of the system diameter for (a) $j_e = 7 \times 10^{10}\mathrm{Am}^{-2}$ and (b) $j_e = 5 \times 10^{11}\mathrm{Am}^{-2}$ at $T = 0\,\mathrm{K}$ (dark colors) and $T = 300\,\mathrm{K}$ (light colors). The error bars are the standard deviation of the switching times calculated over ten independent switching events. The inset in (b) is a sketch to show the division of the total switching time in transient and reversal components.

distribution approaches a value close to that of the reversal time for large current densities. Separating the switching time into reversal and transient components allows us to distinguish between intrinsic and extrinsic factors contributing to the magnetization dynamics induced by the spin-polarized current. Hence, we believe that such an approach can be a useful tool to optimize the switching dynamics by focusing on the specific targets.

C. Comparison with experiments

Devolder *et al.* [36,37] and Hahn *et al.* [38] have performed time-resolved spin transfer torque switching experiments on CoFeB/MgO-based MTJs. Devolder and collaborators measured switching events as a function of MTJ diameter and applied voltage and found that the reversal of the magnetization occurs via reversed-domain nucleation and wall propagation through the system with a linear propagation of the reversed region from one edge to the other. In similar studies, Hahn *et al.* [38] find that the switching time is more sensitive to the lateral size of the stack at low current densities and that the switching is domain wall mediated, followed by linear propagation. Because of a more complex dynamics when switching from antiparallel to parallel configuration, Hahn *et al.* attribute the change to a different reversal mechanism. Our simulations agree with the results presented in Ref. [38] showing a stronger dependence on the diameter of the MTJ when low current densities are injected. Similarly, the conclusion drawn by both Devolder *et al.* and Hahn *et al.*, namely that reversal is nonuniform, is supported by our simulations for similar MTJ diameters. However, our results are characterized by a rotation of the reversed region in addition to the propagation, something not observed experimentally. Experimentally accessing the nano- or subnanotimescale is extremely challenging, and hence it is perhaps not surprising that such features have not been registered in the experimental measurements. Micromagnetic simulations are difficult in systems thick enough that the magnetic properties are not uniform in the perpendicular direction and where surface and thermal effects are important. Therefore, simulations of spin-polarized induced magnetization dynamics by means of atomistic spin modeling are able to predict the switching dynamics. Atomistic spin modeling can thus shine some light on the reversal mechanism and be a useful model to interpret experimental results, even in its simplest form derived from a macroscopic theory.

VI. CONCLUSIONS

We have simulated the magnetization dynamics induced by the injection of spin-polarized currents into a CoFeB/MgO/CoFeB magnetic tunnel junction. We have used an atomistic spin model where the spin transfer torque is modeled based on Slonczewski's approach and parametrized following the work of Zhang, Levy, and Fert [14]. To aid the analysis of the switching dynamics driven by spin transfer torque, we have exploited excitation modes and a newly defined contour integral of the magnetization. Our results show that the magnetization reversal is driven by the combination of coherent and nonuniform excitation modes that, depending on the lateral size, temperature, and injected current density, can be either nonuniform and initiated by a coherent mode of the magnetization, or domain wall nucleated. These results present comparable features to those of experimental measurements of spin transfer torque switching in similar CoFeB/MgO-based magnetic tunnel junctions. Moreover, the simulations suggest a more complex switching dynamics than usually assumed both experimentally and theoretically, and they show the need for accurate modeling of the spin torque phenomenon. Larger injected currents result in stronger excitation of nonuniform modes. This is not desirable on the device level as it makes the switching more easily subjected to structural imperfections, such as edge damages, or thermal excitations. To reduce the operational writing time of a MTJ, the transient time would need to be reduced as it represents the incubation time. In addition, making the transient time shorter would allow to reduce the stochasticity of the switching process since this period is strongly affected by temperature. As a final remark, we believe that to obtain a deeper understanding of spin transfer torque induced magnetization dynamics, more accurate and detailed modeling, such as the spin accumulation model discussed in Ref. [15], should be used.

ACKNOWLEDGMENTS

The authors gratefully acknowledge funding from the Samsung SGMI programme. The authors would like to thank the York Advanced Computing Cluster (YARCC) for access to computational resources.

[1] S. Ikeda, J. Hayakawa, Y. M. Lee, F. Matsukura, Y. Ohno, T. Hanyu, and H. Ohno, IEEE Trans. Electron Dev. **54**, 991 (2007).

[2] B. Dieny, R. B. Goldfarb, and K. J. Lee, *Introduction to Magnetic Random-Access Memory* (Wiley-IEEE Press, 2016).

[3] S. Bhatti, R. Sbiaa, A. Hirohata, H. Ohno, S. Fukami, and S. Piramanayagam, Mater. Today **20**, 530 (2017).

[4] J. Slonczewski, J. Magn. Magn. Mater. **159**, L1 (1996).

[5] C. Chappert, A. Fert, and F. N. V. Dau, Nat. Mater. **6**, 813 (2007).

[6] A. V. Khvalkovskiy, D. Apalkov, S. Watts, R. Chepulskii, R. S. Beach, A. Ong, X. Tang, A. Driskill-Smith, W. H. Butler, P. B. Visscher, D. Lottis, E. Chen, V. Nikitin, and M. Krounbi, J. Phys. D **46**, 139601 (2013).

[7] P. H. Jang, K. Song, S. J. Lee, S. W. Lee, and K. J. Lee, Appl. Phys. Lett. **107**, 202401 (2015).

[8] K. Munira and P. B. Visscher, J. Appl. Phys. **117**, 17B710 (2015).

[9] J. Sampaio, A. V. Khvalkovskiy, M. Kuteifan, M. Cubukcu, D. Apalkov, V. Lomakin, V. Cros, and N. Reyren, Appl. Phys. Lett. **108**, 112403 (2016).

[10] P. B. Visscher, K. Munira, and R. J. Rosati, arXiv:1604.03992.

[11] P. Bouquin, S. Rao, G. S. Kar, and T. Devolder, Appl. Phys. Lett. **113**, 222408 (2018).

[12] J. B. Mohammadi and A. D. Kent, arXiv:2003.13875.

[13] A. Meo, P. Chureemart, S. Wang, R. Chepulskyy, D. Apalkov, R. W. Chantrell, and R. F. L. Evans, Sci. Rep. **7**, 16729 (2017).

[14] S. Zhang, P. M. Levy, and A. Fert, Phys. Rev. Lett. **88**, 236601 (2002).

[15] P. Chureemart, I. D'Amico, and R. W. Chantrell, J. Phys.: Condens. Matter **27**, 146004 (2015).

[16] "Computer code VAMPIRE 5.0" (2019).

[17] R. F. L. Evans, W. J. Fan, P. Chureemart, M. O. A. Ellis, T. A. Ostler, and R. W. Chantrell, J. Phys.: Condens. Matter **26**, 103202 (2014).

[18] M. O. A. Ellis, R. F. L. Evans, T. A. Ostler, J. Barker, U. Atxitia, O. Chubykalo-Fesenko, and R. W. Chantrell, Low Temp. Phys. **41**, 705 (2015).

[19] S. Jenkins, A. Meo, L. E. Elliott, S. K. Piotrowski, M. Bapna, R. W. Chantrell, S. A. Majetich, and R. F. L. Evans, J. Phys. D: Appl. Phys. **53**, 044001 (2020).

[20] G. J. Bowden, G. B. G. Stenning, and G. van der Laan, J. Phys.: Condens. Matter **28**, 066001 (2016).

[21] M. Fähnle and C. Illg, J. Phys.: Condens. Matter **23**, 493201 (2011).

[22] P. M. Levy, J. Phys. D **35**, 2448 (2002).

[23] Z. Li and S. Zhang, Phys. Rev. B **68**, 024404 (2003).

[24] S. Zhang and Z. Li, Phys. Rev. Lett. **93**, 127204 (2004).

[25] C. Burrowes, A. P. Mihai, D. Ravelosona, J.-V. Kim, C. Chappert, L. Vila, A. Marty, Y. Samson, F. Garcia-Sanchez, L. D. Buda-Prejbeanu, I. Tudosa, E. E. Fullerton, and J.-P. Attané, Nat. Phys. **6**, 17 (2010).

[26] T. Taniguchi, S. Yakata, H. Imamura, and Y. Ando, Appl. Phys. Express **1**, 031302 (2008).

[27] H. Sato, P. Chureemart, F. Matsukura, R. W. Chantrell, H. Ohno, and R. F. L. Evans, Phys. Rev. B **98**, 214428 (2018).

[28] S. Ikeda, K. Miura, H. Yamamoto, K. Mizunuma, H. D. Gan, M. Endo, S. Kanai, J. Hayakawa, F. Matsukura, and H. Ohno, Nat. Mater. **9**, 721 (2010).

[29] D. A. Garanin, Phys. Rev. B **53**, 11593 (1996).

[30] D. Jiles, *Introduction to Magnetism and Magnetic Materials* (Chapman and Hall, London, 1991).

[31] A. Aharoni, *Introduction to the Theory of Ferromagnetism*, International Series of Monographs on Physics Vol. 109, 2nd ed. (Oxford University Press, Oxford, 1996).

[32] R. Skomski, *Simple Models of Magnetism* (Oxford University Press, Oxford, 2008), p. 365.

[33] T. Devolder, J.-V. Kim, L. Nistor, R. Sousa, B. Rodmacq, and B. Diény, J. Appl. Phys. **120**, 183902 (2016).

[34] T. Devolder, P.-H. Ducrot, J.-P. Adam, I. Barisic, N. Vernier, J.-V. Kim, B. Ockert, and D. Ravelosona, Appl. Phys. Lett. **102**, 022407 (2013).

[35] S. Sampan-a-pai, J. Chureemart, R. W. Chantrell, R. Chepulskyy, S. Wang, D. Apalkov, R. F. L. Evans, and P. Chureemart, Phys. Rev. Appl. **11**, 044001 (2019).

[36] T. Devolder, J.-V. Kim, F. Garcia-Sanchez, J. Swerts, W. Kim, S. Couet, G. Kar, and A. Furnemont, Phys. Rev. B **93**, 024420 (2016).

[37] T. Devolder, A. Le Goff, and V. Nikitin, Phys. Rev. B **93**, 224432 (2016).

[38] C. Hahn, G. Wolf, B. Kardasz, S. Watts, M. Pinarbasi, and A. D. Kent, Phys. Rev. B **94**, 214432 (2016).